Electronic Supplementary Material (ESI) for Physical Chemistry Chemical Physics.


# Supporting information

# for

# Influence of riboflavin on oxidation kinetics of unsaturated fatty acids at the air/aqueous interface revealed by sum frequency generation vibrational spectroscopy

Yingxue Ma,[a,b] Jian Hou,[a,b] Wenying Hao,[a,b] Jianchuan Liu,[a,b] Lingwei Meng,[a,b] Zhou Lu*[,a,b]

[a] Beijing National Laboratory for Molecular Sciences, CAS Research/Education Center for Excellence in Molecular Sciences, Institute of Chemistry, Chinese Academy of Sciences, Beijing 100190, China.

[b] University of Chinese Academy of Sciences, Beijing 100049, China.

* E-mail: zhoulu@iccas.ac.cn

## 1. The spectral resolutions of SFG-VS

Two different types of the sum frequency generation vibrational spectroscopy (SFG-VS) apparatuses, one was based on a 33 ps Nd:YAG laser system running at the scanning mode and the other is a high-resolution broadband SFG-VS (HR-BB-SFG-VS) spectrometer, were used in current study.

In the scanning-mode SFG-VS setup, the bandwidth of the IR beam instead of that of the visible beam determines the spectral resolutions. This is because that both the visible and IR beams in the scanning SFG-VS systems have narrow bandwidths and the PMT detector collected all the SFG-VS signals nearby the SFG wavelength. The visible beam in our scanning SFG-VS system was based on the frequency doubling of the 1064 nm laser output with a pulse width of 33 ps. The corresponding FWHM bandwidth is about 0.32 $cm^{-1}$ assuming a $sech^2$ pulse. On the other hand, the IR beam was produced by the difference frequency generation between idler beam from the optical parametric amplifications and the 1064 nm fundamental beam. The IR bandwidth was therefore determined by the bandwidth of the idler beam. The latter was a result of dispersing the idler light by an optical grating and the following wavelength selection by a small pinhole. The resultant IR bandwidth then varied between 2 $cm^{-1}$ and 6 $cm^{-1}$ in our setup, depending on the wavelength. As a result, the SFG-VS resolution of such a scanning SFG-VS setup was mainly decided by the IR bandwidth that was broader than that of the 532 nm visible beam. The SFG-VS resolution was wavelength dependent since the IR bandwidth was wavelength dependent. In our setup, a resolution of 6 $cm^{-1}$ can be achieved across the 1000-4000 $cm^{-1}$ range. Around 3000 $cm^{-1}$, this resolution was around 2 $cm^{-1}$.[1-6]

The HR-BB-SFG-VS belongs to the category of multiplex-mode broadband SFG-VS. The IR beam is based on a femtosecond pulses which typically covers a bandwidth of several hundred wavelength, therefore one does not need to scan the IR wavelength during the experiment. Instead, the broadband IR pulse directly overlaps with a narrowband visible beam to generate the SFG-VS signals which are spectrally resolved by using the spectrograph to disperse the SFG signal light onto a CCD camera. In such setups, the key to achieve the better spectral resolutions is to have the bandwidth of visible beam as narrow as possible. In current work, we employed a 50 ps laser pule centered at 800 nm as the visible beam. The corresponding visible bandwidth is therefore only 0.21 $cm^{-1}$. This together with the small pixel size (16 × 16 $\mu m^2$) of CCD and the long focal length (750 mm) of the spectrograph made the sub-1 $cm^{-1}$ spectral resolution possible. In fact, a spectral resolution as high as 0.4 $cm^{-1}$ can be achieved with a 1800 l/mm grating in this setup. In current work a 1200 l/mm grating as used. The measured spectral resolution was 0.6 $cm^{-1}$.

## 2. Fitting of SFG-VS spectra

The SFG signal intensity $I_{SF}$ is given by[7, 8]

$$I_{SF} \propto \left|\chi_{eff}\right|^2 I_{vis}(\omega_{vis}) I_{IR}(\omega_{IR}) \qquad \text{(Eq. S1)}$$

where $I_{vis}(\omega_{vis})$ $\chi_{eff}$ is the effective second order susceptibility and can be expressed as

$$\chi_{eff} \propto \chi_{NR} + \sum_q \frac{A_q}{\omega_{IR} - \omega_q + i\Gamma_q} \qquad \text{(Eq. S2)}$$

In equation (2), $\chi_{NR}$ denotes the non-resonant term. $A_q$, $\omega_q$ and $\Gamma_q$ represent the sum frequency strength factor tensor, resonant frequency and damping constant of the qth vibrational mode, respectively.

The above equations were used to fit the SFG-VS spetra in the work.

## 3. Control experiments

Figure S1 shows the high-resolution broadband sum frequency generation vibrational spectra (HR-BB-SFG-VS) of EA monolayer at the air/neat water interface with MMA=35 Å$^2$. The spectra were taken with there different polarization combinations (ssp, ppp and sps) and under the protection of nitrogen purging gas. A detailed comparison between the ssp/sps and ppp spectra shows a spectral splitting in the $CH_2$ symmetric stretching region, the origin of which is still under the investigation. A weak vinyl =CH stretching peak around 3017 cm$^{-1}$ was also observed in the ssp spectrum.[9] Besides the ssp peak we already mentioned in the main text, a broad $CH_2$ asymmetric stretching peak around ~2891 cm$^{-1}$ were observed in both the ppp and sps spectra. In addition, a 2~3 cm$^{-1}$ splitting between the sps and ppp spectra can be seen in the $CH_3$ antisymmetric stretching region around 2965 cm$^{-1}$. This spectral splitting can be attributed to the splitting of the in-plane and out-of-plane $CH_3$ antisymmetric stretching as we previously reported.[10]

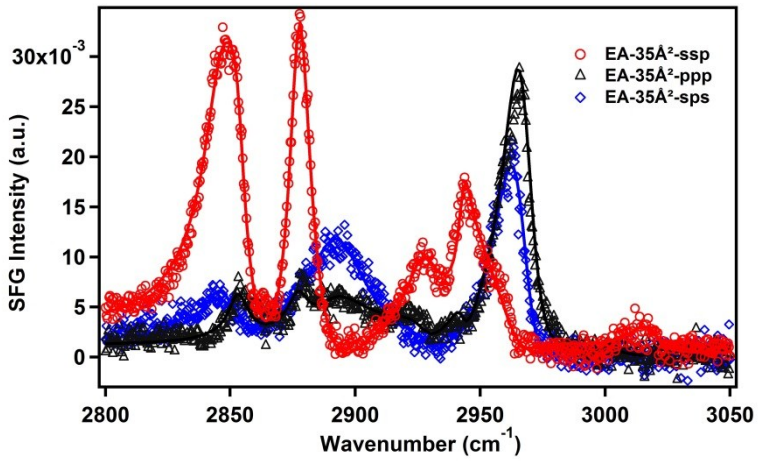


**Figure S1** The high-resolution broadband sum frequency generation vibrational spectra of EA monolayer at the air/neat water interface with MMA=35 Å$^2$/molecule under the ssp, ppp and sps polarization combinations.

Figure S2 displays the SFG-VS spectra of the EA monolayer (MMA=35 Å$^2$) at the air/neat water interface under the protection of nitrogen. It clearly shows that after 150 min's purging with nitrogen, the SFG-VS spectra still remained unchanged, confirming that the changes observed in the spectra plotted in Figure 2 were from the oxidation of EA monolayer in the air.

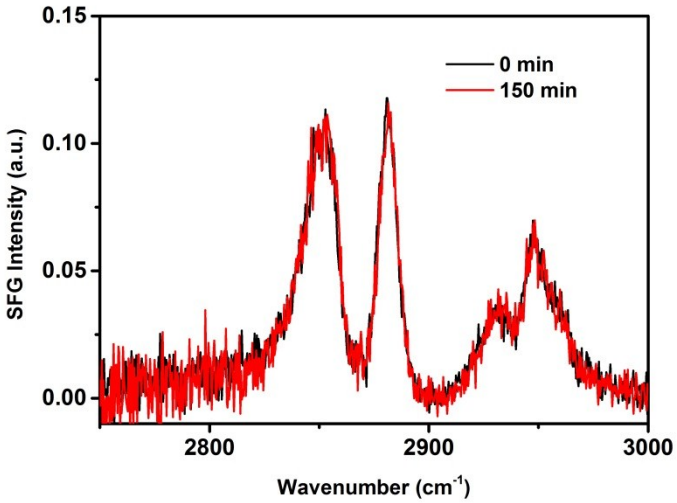


**Figure S2** The HR-BB-SFG spectra of EA monolayer before and after the 150-min nitrogen purging. The EA monolayer was spread at the air/neat water interface with MMA=35 Å$^2$. The spectra were obtained under the ssp polarization combination.

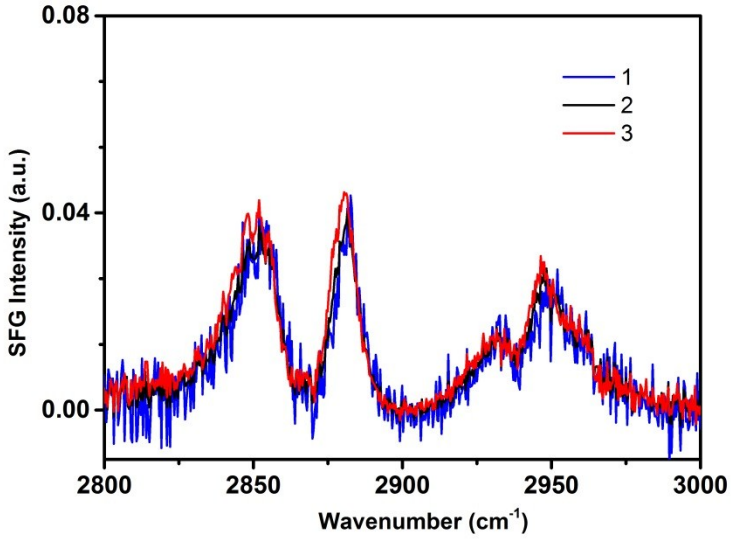


**Figure S3** The HR-BB-SFG spectra of several EA monolayer independently prepared at different times but with the same conditions at the air/neat water interfaces. The MMA=35 Å$^2$/molecule. The spectra were taken under the protection of nitrogen purging gas and with the ssp polarization. It can be seen that the reproducibility was reasonably good between different measurements.

## 4. Oxidation kinetics monitored by the time-dependent surface pressure decay

The oxidation kinetics was also monitored by the surface pressure measurements. It can be seen from Figure S4 below that the surface pressure is almost linearly proportional to the molecular densities of EA within the range of 3-25 mN/m. Therefore we have

$$\pi = \pi_0 N_s + b, \qquad \text{(Eq. S3)}$$

where $N_s$ is the molecular number density at the interface, $\pi$ is the surface pressure, $\pi_0$ is the surface pressure due to the effect of packing of EA molecules, b is a negative constant used to ascribe the rise of surface pressure at EA densities larger than zero.

As shown in Figure S4, Eq. S3 is valid roughly within the range of surface pressures that we are interested in for the current study. Combining Eq. S3 as well as Eq. 2, we can fit the time-dependent decay of surface pressures in Figure 5 of the main text to obtain the oxidation rate constants.

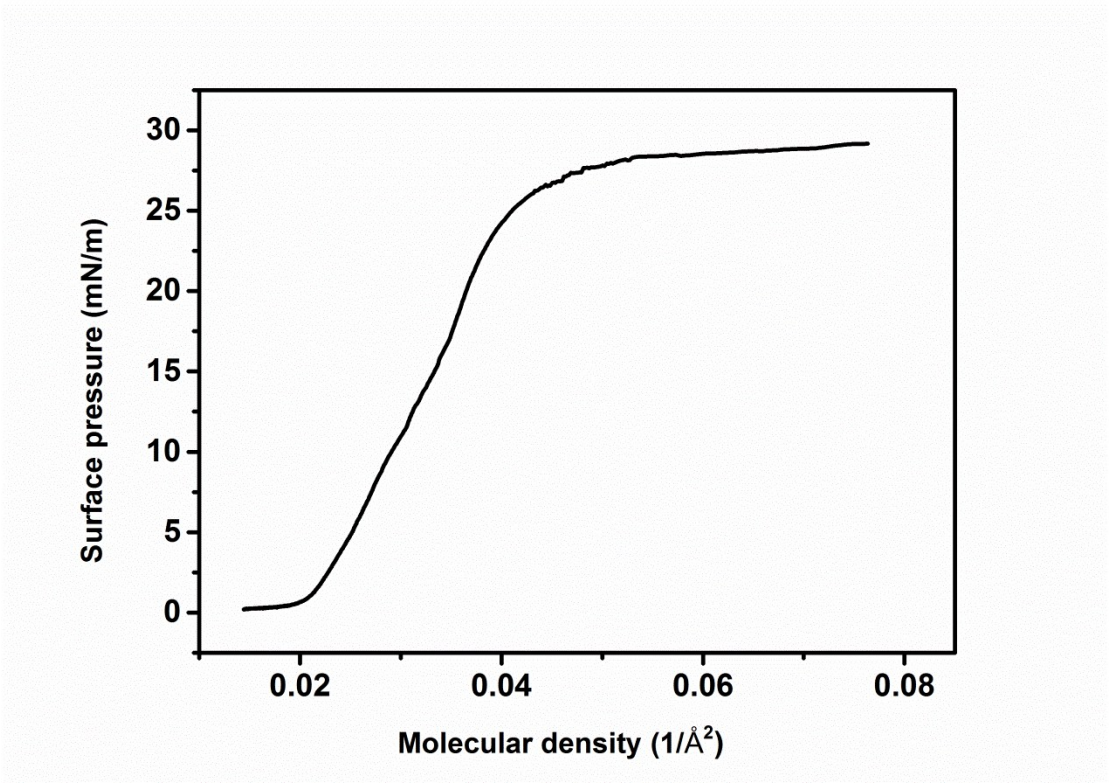


**Figure S4** The surface pressure as a function of surface molecular density for EA on pure water subphase.

## References


1. A. Saha, S. SenGupta, A. Kumar and P. D. Naik, *J. Phys. Chem. C*, 2017, **121**, 13175.
2. F. Wei, W. Xiong, W. Li, W. Lu, H. C. Allen and W. Zheng, *Phys. Chem. Chem. Phys.*, 2015, **17**, 25114.
3. G. Deng, Y. Guo, X. Li, Z. Zhang, S. Liu, Z. Lu and Y. Guo, *Sci. Chin. Chem.*, 2015, **58**, 439.
4. M. J. Hofmann and P. Koelsch, *J. Chem. Phys.*, 2015, **143**, 134112.
5. X. Li, G.H. Deng, R.J. Feng, K. Lin, Z. Zhang, Y. Bai, Z. Lu and Y. Guo, *Chin. Chem. Lett.*, 2016, **27**, 535.
6. G. Deng, X. Li, Y.q. Guo, S.l. Liu, Z. Lu and Y. Guo, *Chin. J. Chem. Phys,* 2013, **26**, 569.
7. H. F. Wang, W. Gan, R. Lu, Y. Rao and B. H. Wu, *Int. Rev. Phys. Chem.*, 2005, **24**, 191.
8. L. Fu, Y. Zhang, Z.H. Wei and H.F. Wang, *Chirality*, 2014, **26**, 509.
9. E. Tyrode, P. Niga, M. Johnson and M. W. Rutland, *Langmuir*, 2010, **26**, 14024.
10. R. J. Feng, X. Li, Z. Zhang, Z. Lu and Y. Guo, *J. Chem. Phys.*, 2016, **145**, 244707.